JOURNAL OF PETROLOGY | VOLUME 44 | NUMBER 1 | PAGES 141–157 | 2003

# Late Palaeozoic Ultramafic Lavas in Yunnan, SW China, and their Geodynamic Significance

**NIANQIAO FANG[1] AND YAOLING NIU[2]***

[1]INSTITUTE OF MARINE GEOLOGY, CHINA UNIVERSITY OF GEOSCIENCES, 29 XUEYUAN ROAD, BEIJING 100083, P.R. CHINA

[2]DEPARTMENT OF EARTH SCIENCES, CARDIFF UNIVERSITY, PO BOX 914, CARDIFF CF10 3YE, UK

**RECEIVED JANUARY 21, 2002; REVISED TYPESCRIPT ACCEPTED JULY 22, 2002**

*We report petrological and geochemical data on ultramafic pillow lavas from Late Palaeozoic marine sequences in Yunnan, SW China. These lavas have >26 wt % MgO, euhedral to subhedral olivine phenocrysts and acicular or quench clinopyroxene crystals with or without microlitic plagioclase in a devitrified and altered glassy matrix. These ultramafic lavas are compositionally komatiitic (>18 wt % MgO), but we term them high-Mg picrites because they lack spinifex-textured olivine. Although olivines in these picrites are cumulate crystals, causing the high MgO contents of the bulk rocks, the high forsterite content of these olivines, Fo = 0·902 ± 0·011, suggests that the primitive magmas parental to the picrites would have had ~17–19% MgO, which is similar to the estimates for primary magmas of the Cretaceous Gorgona komatiites in the literature. The calculated liquidus temperature of the primitive magmas parental to the Yunnan picrites is ~1400 ± 25°C, which would imply a mantle potential temperature of ~1540 ± 30°C. This is inconsistent with magma generation beneath ocean ridges or in the mantle wedge above a subduction zone, but is consistent with a mantle plume origin, which is fully supported by the trace element characteristics of the magmas.*

KEY WORDS: *komatiites; picrites; China; mantle plumes*

## INTRODUCTION

Ultramafic lavas that may be termed komatiites or high-magnesian picrites are widespread in Late Palaeozoic marine sequences within several orogenic belts in Yunnan, SW China (Figs 1 and 2; Fang *et al.*, 1996). These lavas have been interpreted to be oceanic plateaux or seamount eruptive rocks associated with mantle plumes or hotspots in the Palaeo-Tethys ocean basin. The plateau lavas are thought to have been accreted onto the existing continents as a result of continental collision during the long and complex evolutionary history of the Tethys ocean basins before the ultimate amalgamation of Eurasia and Gondwana in the Tertiary (Fang *et al.*, 1996). Given the fact that ultramafic lavas (i.e. komatiites or high-magnesian picrites) are very high temperature mantle melts that are common in the Archaean, but rare in the Phanerozoic (Arndt & Nisbet, 1982), except for those of Cretaceous age found on Gorgona Island (e.g. Echeverria, 1982; Kerr *et al.*, 1996; Arndt *et al.*, 1997; Révillon *et al.*, 2000), it is important that these Late Palaeozoic ultramafic lavas in SW China are carefully examined. The ultramafic lavas appear to have been erupted under submarine conditions and exhibit well-preserved pillow structures (Fig. 3). Despite the widespread occurrence of the picrites (Fig. 1), the outcrops are rather sparse because of neotectonic complications (e.g. effects of India–Eurasia collision and the uplift of the Tibetan plateau) and because of the extensive vegetation in the region. In this contribution, we discuss the petrography, mineral compositions, and whole-rock major and trace element geochemistry of seven representative samples: six ultramafic lavas and one basaltic lava. We also discuss briefly their petrogenesis and geochemical implications. It is our intention that this short paper will draw the attention of

*Corresponding author. Telephone: 44-29-2087-6411. Fax: 44-29-2087-4326. E-mail: NiuY@Cardiff.ac.uk

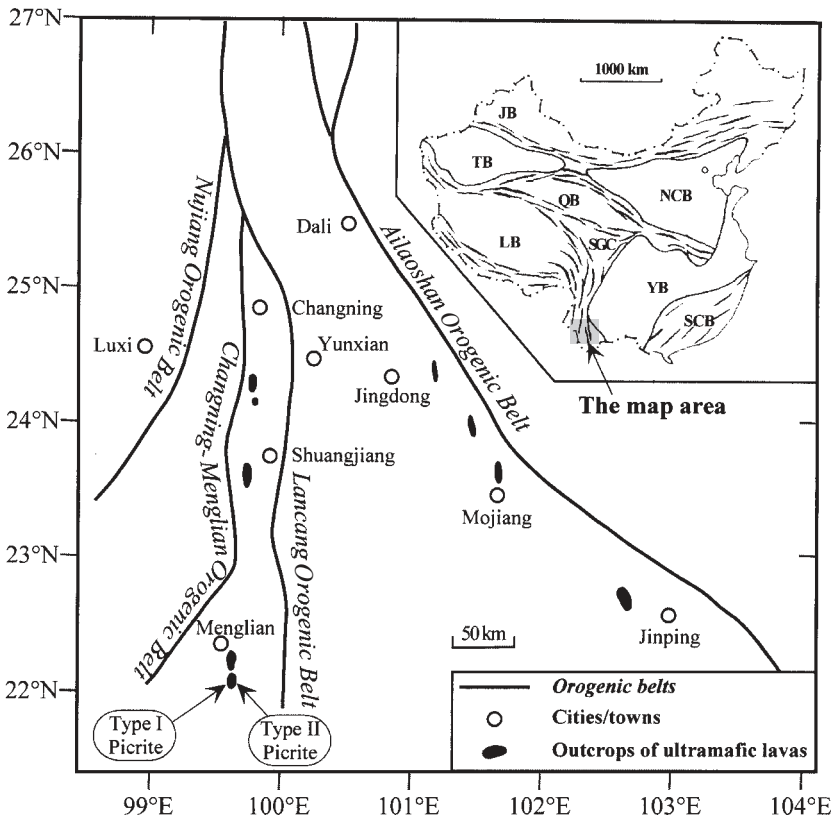


**Fig. 1.** Outcrops of ultramafic lavas in Yunnan, SW China, with regional tectonic framework shown by several orogenic belts (after Fang *et al.*, 1996). Each indicated 'outcrop' represents a cluster of many smaller individual outcrops. Type I and Type II picrites, which both are from the southernmost 'outcrop', are in fact from two tectonic slices separated by a fault zone marked by the Nanlei river (too small to show on the map). The inset (after Wang & Mo, 1995) shows the study area in the context of a geological sketch of mainland China, in which distinct tectonic blocks (abbreviated letters) are separated by complex orogenic belts marked by bold discontinuous lines. TB, Tarim Block (Tarim basin); JB, Junggar Basin; QB, Qaidam Block; NCB, North China Block; LB, Lhasa Block; SGC, Songpan–Ganzi Complex; YB, Yangzi Block; SCB, South China Block.

the international community to these rocks and encourage more detailed research in the context of global tectonics and the Earth's thermal evolution.

## SAMPLES AND BRIEF PETROGRAPHY

The samples studied were taken from outcrops near Menglian (Fig. 1), where both ultramafic and basaltic pillow lavas are abundant. These lavas are locally intercalated with radiolarian cherts and stratigraphically overlain by shallow-water limestones (Fig. 2). Radiolaria in the intercalated cherts of Menglian and from other outcrops in the region (Fig. 1) suggest eruption ages varying from early to late Carboniferous, about a 50–60 Myr time span (Fig. 2; Fang *et al.*, 1996). It is clear that not all these ultramafic lavas are related to a single magmatic event although we recognize that many mantle plumes are long lived (e.g. >80 Myr for Hawaii and >60 Myr for Iceland). Obviously, high-precision geochronology is required to place good time constraints.

Figure 4 shows photomicrographs of representative samples of the Yunnan ultramafic lavas. The samples are all altered to various extents with loss on ignition varying from 5·2 to 10·8 wt %. Texturally, the six ultramafic lavas can be grouped into two types. These two types occur in close geographical proximity, separated by a small river, the Nanlei River, interpreted to be a local fault zone. Type I picrites (YN14a, YN14b and YN16 from west of the Nanlei River) are somewhat altered. The primary mineralogy is dominated by anhedral (most) or subhedral (some) olivine phenocrysts of variable size (0·5–3 mm) with abundant fractures filled with serpentine, chlorite and other alteration products. Clinopyroxene occurs mostly as quench blades or elongated prisms of up to 2 mm in length. Quench plagioclase needles or blades are also present in all thin sections up to 1·5 mm

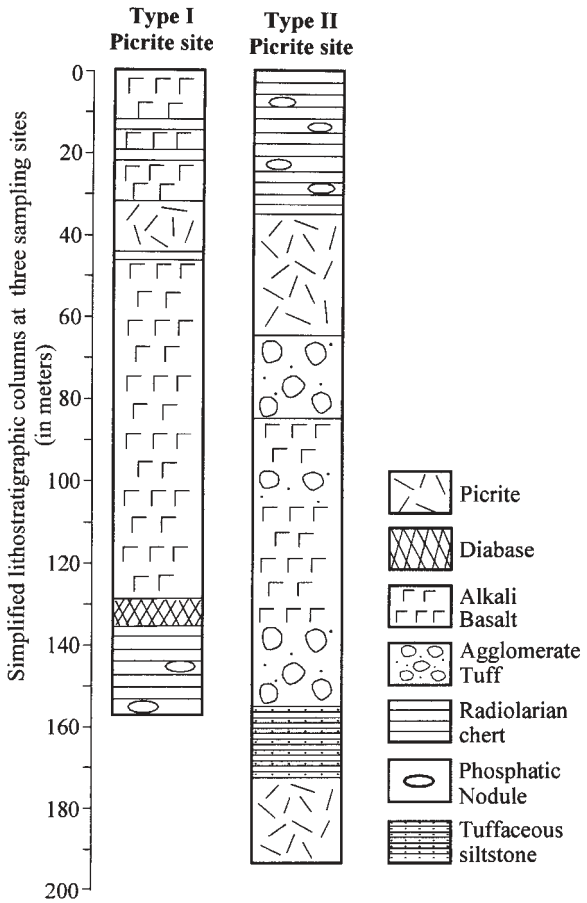


**Fig. 2.** Simplified stratigraphic columns for the two sample sites. The intercalated chert in Type I picrite site (samples YN14a, YN14b, YN16) contains radiolarians (*Pseudoalbaillella annulata* Ishiga, *Provisocyntra pskemensis* Nazarov et Ormiston, *Archocyrtium coronaesimile* Won, *Robotium* sp.) that give a Late Carboniferous age. The intercalated chert in Type II picrite site (samples YN17, MXE441, MXE01 and also basalt YN18) contains radiolarians (*Albaillella deflandrei* Gourmelon, *A. paradoxa* Deflandre, *Entactinia vugaris* Won) that give an Early Carboniferous age. It should be noted that shallow-water limestones stratigraphically above the columns are not shown.

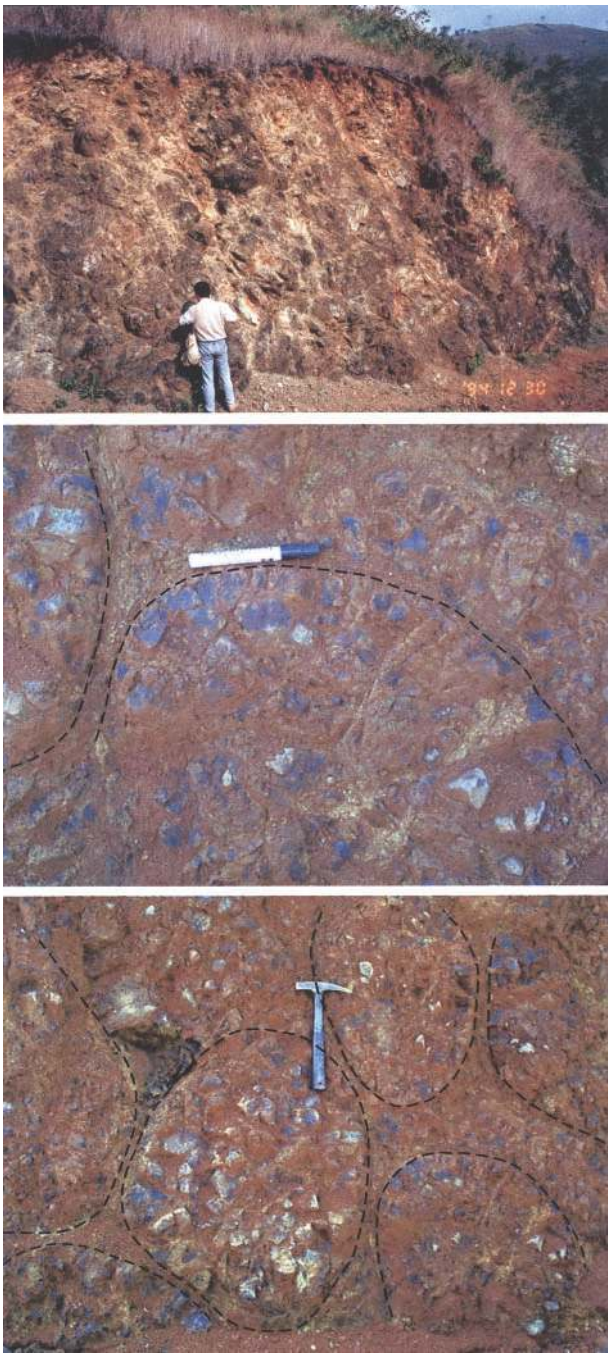

**Fig. 3.** Photographs of ultramafic pillows along road cuts south of Menglian (Fig. 1, Type I picrite site). Bottom two panels are close-ups, in which the dashed black lines mark the outlines of the pillows. The scales are denoted by the marker pen (14 cm long, middle) and geological hammer (29 cm long, bottom).

long. The least abundant are euhedral or subhedral spinel crystals. The groundmass, which is interpreted to be devitrified glass, is volumetrically <30%, and is mostly made up of secondary chlorite and minor actinolite–tremolite and serpentine. Vesicles of up to 3 mm in diameter are present in all thin sections, suggesting volatile-rich melts or eruption in shallow water depth.

Type II picrites (YN17, MXE441 and MXE01 from east of the Nanlei River) are also altered. The primary mineralogy is dominated by euhedral olivine phenocrysts of variable size (0·5–3 mm). The olivine crystals are less fractured than Type I olivines, but altered to various extents to chlorite with fresh cores preserved. Clinopyroxene occurs as quench needles or blades or rarely as small (<0·5 mm) euhedral–subhedral crystals, some displaying spinifex texture. No plagioclase quench crystals are observed in Type II picrites. The groundmass is devitrified glass replaced mostly by chlorite, and to a lesser extent by tremolite and serpentine. Small euhedral–subhedral spinel crystals are present. Vesicles are also

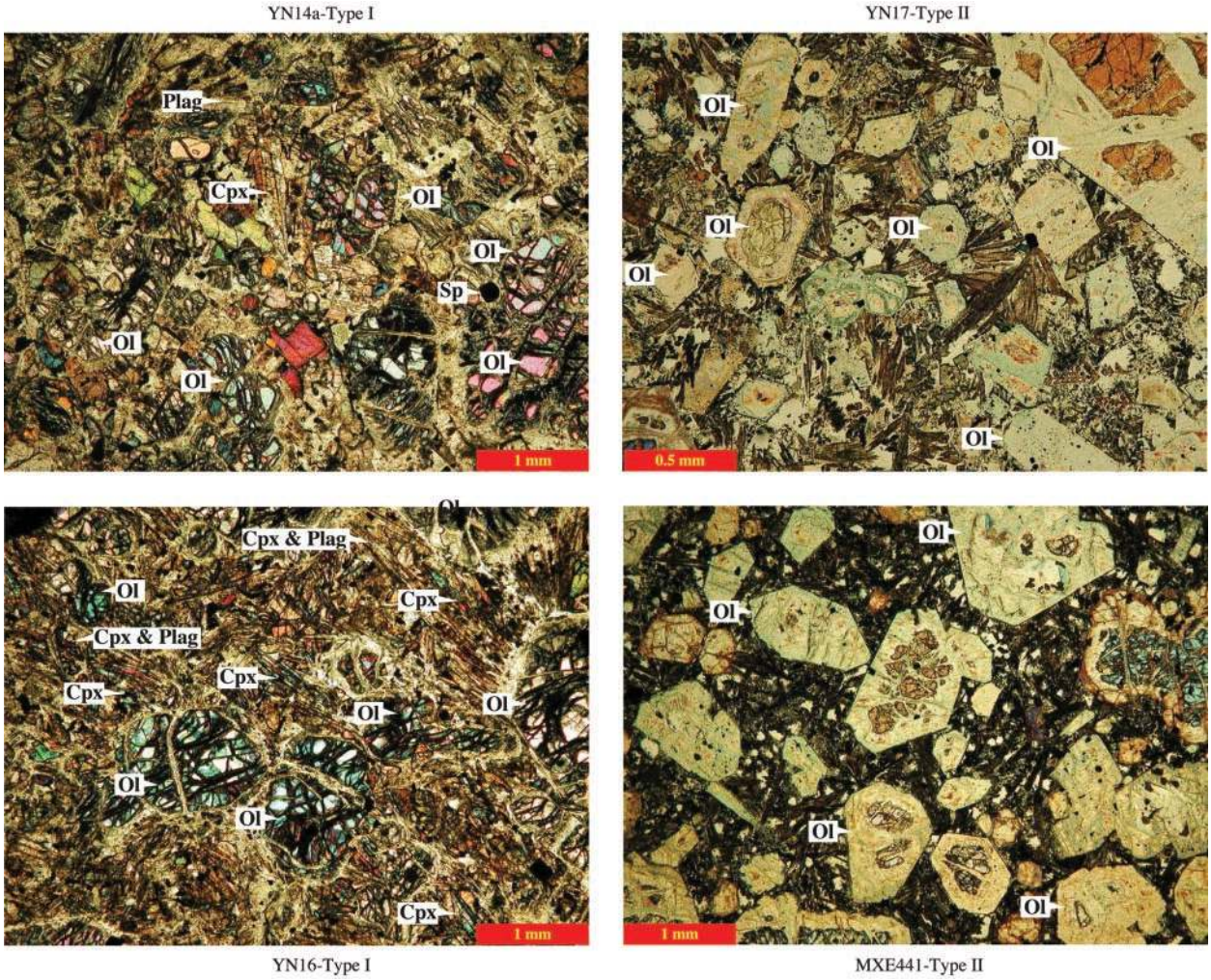


**Fig. 4.** Photomicrographs of representative Type I and Type II picrite lavas, all taken under cross-polarized light. Ol, olivine phenocrysts; Cpx, clinopyroxene quench crystals; Plag, plagioclase quench microlites; Sp, spinel.

present in Type II picrites. It should be noted that the two textural types also differ in geochemistry (see below).

## ANALYTICAL METHODS AND DATA

Major and minor element compositions (Si, Ti, Al, Fe, Mn, Mg, Ca, Na, K, P, Cr and Ni) of phenocryst olivine, quench clinopyroxene, quench plagioclase and small spinel phenocrysts of the Yunnan picrites were analysed on polished thin sections using a JEOL Superprobe JXA-8800L at The University of Queensland. Analytical conditions were optimized for standard silicates and oxides at 15 kV accelerating voltage with a 20 nA focused electron beam for all the elements with the exception of Na and K, for which a broader beam (10 mm) was used. Routine analyses were obtained by counting for 30 s at peak and 5 s on background. Repeated analysis of natural and synthetic mineral standards yielded precisions better than 2% for elements with abundances >5 wt %, and better than 5% for those <5 wt %. Instrumental drift was negligible during the session of the analysis. Averages and standard deviations of major element compositions of phenocryst olivine, quench clinopyroxene, quench plagioclase and small spinel phenocrysts of the picrites are given in Table 1.

Major element oxides ($SiO_2$, $TiO_2$, $Al_2O_3$, FeO, MnO, MgO, CaO, $Na_2O$, $K_2O$ and $P_2O_5$) for whole-rock samples were analysed by inductively coupled plasma-optical emission spectroscopy (ICP-OES) using a Perkin Elmer Optima 3300 DV system at The University of Queensland following the procedure of Kwiecien (1990). Precision ($1\sigma$) for most elements based on US Geological Survey (USGS) rock standards (BCR-1, BIR-1, AGV-1 and G2) is better than 1% with the exception of $TiO_2$ ($\sim$1·5%) and $P_2O_5$ ($\sim$2·0%). Loss on ignition (LOI) was

*Table 1: Average and 1σ standard deviation microprobe analyses of mineral phases in the ultramafic pillow lavas from Yunnan, SW China*

| | Ol | | | | | | Cpx | | | | | | Spinel | | | | | Plag | | |
|---|---|---|---|---|---|---|---|---|---|---|---|---|---|---|---|---|---|---|---|---|
| | Type I picrite | | | Type II picrite | | | Type I picrite | | | Type II picrite | | | Type I picrite | | Type II picrite | | | Type I picrite | | |
| | YN14a | YN14b | YN16 | YN17 | MXE441 | MXE01 | YN14a | YN14b | YN16 | YN17 | MXE441 | MXE01 | YN14a | YN16 | YN17 | MXE441 | MXE01 | YN14a | YN14b | YN16 |
| *n*: | 8 | 5 | 5 | 5 | 10 | 9 | 15 | 7 | 15 | 5 | 7 | 8 | 5 | 15 | 5 | 5 | 5 | 5 | 5 | 10 |
| $SiO_2$ | 40·49 | 40·78 | 40·75 | 40·46 | 40·30 | 40·32 | 50·31 | 49·39 | 49·50 | 44·56 | 44·77 | 51·44 | 0·139 | 0·104 | 0·082 | 0·057 | 0·077 | 49·29 | 48·78 | 50·33 |
| 1σ | 0·402 | 0·268 | 0·065 | 0·223 | 0·562 | 0·428 | 0·372 | 0·502 | 1·001 | 1·189 | 0·672 | 1·317 | 0·011 | 0·070 | 0·019 | 0·011 | 0·006 | 2·243 | 2·173 | 0·587 |
| $TiO_2$ | 0·007 | 0·004 | 0·006 | 0·015 | 0·013 | 0·012 | 1·124 | 1·324 | 1·341 | 3·324 | 3·033 | 1·115 | 0·377 | 0·387 | 1·631 | 2·766 | 1·670 | 0·061 | 0·041 | 0·062 |
| 1σ | 0·006 | 0·009 | 0·010 | 0·011 | 0·010 | 0·009 | 0·146 | 0·238 | 0·386 | 0·658 | 0·622 | 0·376 | 0·032 | 0·106 | 0·304 | 0·172 | 0·092 | 0·010 | 0·025 | 0·019 |
| $Al_2O_3$ | 0·101 | 0·086 | 0·078 | 0·061 | 0·051 | 0·045 | 4·699 | 5·464 | 5·186 | 9·121 | 9·314 | 3·364 | 25·86 | 30·70 | 14·96 | 17·26 | 14·12 | 29·62 | 29·73 | 30·34 |
| 1σ | 0·016 | 0·012 | 0·013 | 0·008 | 0·009 | 0·014 | 0·473 | 0·821 | 1·319 | 0·400 | 0·363 | 1·177 | 0·199 | 4·737 | 0·666 | 0·126 | 0·202 | 1·135 | 0·844 | 0·461 |
| FeOt | 9·452 | 7·933 | 8·758 | 9·910 | 10·271 | 10·717 | 7·825 | 8·343 | 9·083 | 10·036 | 9·746 | 5·983 | 13·62 | 16·22 | 23·10 | 31·95 | 22·26 | 3·010 | 1·788 | 1·161 |
| 1σ | 0·418 | 0·098 | 0·078 | 0·103 | 0·284 | 0·413 | 1·343 | 2·332 | 1·146 | 0·509 | 0·591 | 0·516 | 1·152 | 2·569 | 3·972 | 0·660 | 0·702 | 2·491 | 1·339 | 0·493 |
| MnO | 0·139 | 0·125 | 0·124 | 0·135 | 0·145 | 0·148 | 0·175 | 0·195 | 0·205 | 0·143 | 0·151 | 0·142 | 0·207 | 0·199 | 0·260 | 0·270 | 0·241 | 0·066 | 0·070 | 0·013 |
| 1σ | 0·013 | 0·013 | 0·010 | 0·012 | 0·022 | 0·011 | 0·033 | 0·052 | 0·054 | 0·017 | 0·024 | 0·026 | 0·029 | 0·035 | 0·038 | 0·020 | 0·015 | 0·063 | 0·064 | 0·014 |
| MgO | 49·11 | 50·37 | 49·52 | 48·71 | 48·37 | 47·97 | 14·46 | 13·87 | 13·85 | 11·43 | 11·19 | 16·08 | 17·05 | 16·91 | 12·91 | 11·75 | 13·41 | 1·71 | 0·44 | 0·53 |
| 1σ | 0·243 | 0·234 | 0·228 | 0·203 | 0·454 | 0·416 | 0·591 | 0·663 | 1·089 | 1·573 | 0·922 | 0·801 | 0·721 | 1·303 | 1·613 | 0·448 | 0·613 | 1·853 | 0·303 | 0·354 |
| CaO | 0·284 | 0·297 | 0·303 | 0·217 | 0·215 | 0·217 | 20·80 | 20·79 | 20·35 | 20·79 | 21·12 | 20·93 | 0·003 | 0·013 | 0·019 | 0·006 | 0·000 | 13·33 | 16·54 | 14·75 |
| 1σ | 0·008 | 0·005 | 0·014 | 0·013 | 0·014 | 0·014 | 0·485 | 1·007 | 0·833 | 1·338 | 0·605 | 0·168 | 0·006 | 0·020 | 0·031 | 0·008 | 0·000 | 1·324 | 2·122 | 0·432 |
| $Na_2O$ | 0·004 | 0·007 | 0·008 | 0·004 | 0·008 | 0·012 | 0·321 | 0·325 | 0·320 | 0·361 | 0·330 | 0·229 | 0·003 | 0·003 | 0·005 | 0·000 | 0·005 | 2·926 | 2·582 | 2·792 |
| 1σ | 0·009 | 0·005 | 0·011 | 0·004 | 0·009 | 0·026 | 0·059 | 0·070 | 0·050 | 0·046 | 0·022 | 0·030 | 0·007 | 0·007 | 0·012 | 0·000 | 0·005 | 0·743 | 0·641 | 0·195 |
| $K_2O$ | 0·004 | 0·007 | 0·005 | 0·006 | 0·001 | 0·004 | 0·002 | 0·003 | 0·006 | 0·010 | 0·010 | 0·002 | 0·000 | 0·004 | 0·001 | 0·003 | 0·002 | 0·044 | 0·022 | 0·042 |
| 1σ | 0·005 | 0·005 | 0·006 | 0·006 | 0·002 | 0·004 | 0·003 | 0·006 | 0·007 | 0·014 | 0·013 | 0·004 | 0·000 | 0·006 | 0·002 | 0·004 | 0·003 | 0·011 | 0·008 | 0·027 |
| $P_2O_5$ | 0·005 | 0·007 | 0·005 | 0·013 | 0·014 | 0·019 | 0·016 | 0·016 | 0·020 | 0·120 | 0·284 | 0·011 | 0·003 | 0·005 | 0·009 | 0·006 | 0·004 | 0·009 | 0·010 | 0·013 |
| 1σ | 0·007 | 0·005 | 0·011 | 0·014 | 0·016 | 0·013 | 0·013 | 0·016 | 0·013 | 0·074 | 0·247 | 0·011 | 0·005 | 0·009 | 0·012 | 0·009 | 0·006 | 0·007 | 0·007 | 0·017 |
| NiO | 0·351 | 0·361 | 0·321 | 0·426 | 0·465 | 0·422 | 0·031 | 0·024 | 0·015 | 0·028 | 0·014 | 0·049 | 0·280 | 0·205 | 0·243 | 0·225 | 0·287 | 0·003 | 0·009 | 0·004 |
| 1σ | 0·024 | 0·046 | 0·022 | 0·031 | 0·027 | 0·021 | 0·018 | 0·016 | 0·013 | 0·019 | 0·018 | 0·026 | 0·024 | 0·036 | 0·043 | 0·039 | 0·022 | 0·004 | 0·012 | 0·005 |
| $Cr_2O_3$ | 0·111 | 0·104 | 0·056 | 0·115 | 0·092 | 0·084 | 0·243 | 0·226 | 0·121 | 0·076 | 0·087 | 0·593 | 42·36 | 35·24 | 46·69 | 35·74 | 47·86 | 0·001 | 0·007 | 0·002 |
| 1σ | 0·018 | 0·031 | 0·019 | 0·014 | 0·015 | 0·017 | 0·148 | 0·138 | 0·092 | 0·037 | 0·046 | 0·356 | 0·301 | 4·852 | 3·376 | 0·557 | 0·342 | 0·003 | 0·009 | 0·005 |
| | Mg-number | | | | | | | | | | | | Cr-number | | | | | Ca-number | | |
| | 0·903 | 0·919 | 0·910 | 0·898 | 0·894 | 0·889 | 0·767 | 0·750 | 0·731 | 0·668 | 0·671 | 0·827 | 0·524 | 0·437 | 0·676 | 0·581 | 0·695 | 0·716 | 0·780 | 0·745 |
| 1σ | 0·004 | 0·001 | 0·001 | 0·001 | 0·003 | 0·004 | 0·037 | 0·058 | 0·032 | 0·031 | 0·026 | 0·018 | 0·001 | 0·071 | 0·026 | 0·005 | 0·004 | 0·496 | 0·647 | 0·551 |

Ol, phenocryst olivine; Cpx, quench clinopyroxene; Plag, quench plagioclase microlite. FeOt, total Fe reported as FeO. Mg-number = Mg/(Mg + $Fe^{2+}$) assuming total FeO as $Fe^{2+}$ for both Ol and Cpx. Cr-number = Cr/(Cr + Al) in spinel, and Ca-number = Ca/(Ca + Na) in plagioclase.

determined by placing 1 g of samples in a furnace at 1000°C for several hours, cooling in a desiccator and reweighing. Trace and minor element (Li, Be, Sc, Ti, V, Cr, Co, Ni, Cu, Zn, Ga, Rb, Sr, Y, Zr, Nb, Cs, Ba, La, Ce, Pr, Nd, Sm, Eu, Gd, Tb, Dy, Ho, Er, Tm, Yb, Lu, Hf, Ta, Pb, Th and U) abundances in these same samples were analysed by inductively coupled plasma-mass spectrometry (ICP-MS) on a Fisons PQ2$^+$ system at The University of Queensland, with analytical conditions and procedures following Eggins *et al.* (1997) and Niu & Batiza (1997), except for sample digestion, which was carried out using high-pressure bombs to ensure complete digestion–dissolution. Precisions ($1\sigma$) are better than 1–2% for most elements, except for transition metals, for which precisions are better than 2–4% based on repeated analyses of highly depleted basaltic samples such as USGS reference rock standard BIR-1 [see Niu & Batiza (1997) for details]. The analytical data are given in Table 2.

## DISCUSSION

### Picrites vs komatiites

The ultramafic lavas have bulk-rock MgO contents >27·5 wt % (Table 2; analyses recalculated to 100% on an anhydrous basis), well in excess of the lower limit of 18 wt % for komatiites (e.g. Le Bas, 2000, 2001), and thus may be classified as komatiites on the basis of geochemistry. However, the lack of spinifex olivine disqualifies their being classified as komatiites (e.g. Arndt & Nisbet, 1982; Kerr & Arndt, 2001). We thus prefer the term 'high-magnesian picrites' in the subsequent discussion. On the other hand, although proper nomenclature is necessary for communication, and may reflect some physical aspect of the petrogenesis (e.g. the site or depth of crystallization, cooling rate, etc.), here we consider that understanding the composition and temperature of the primary mantle melts is the most important issue. This latter information is essential for evaluating mantle melting conditions and the Earth's thermal evolution (e.g. Nisbet *et al.*, 1993).

### Composition and temperature of parental melts favour a mantle plume origin

Although Type II olivines tend to have lower MgO (but higher NiO) than Type I olivine, they are all on average $\sim Fo_{90}$ (Table 1). This highly magnesian olivine composition contrasts with the much lower Mg-number (0·6–0·82) of the quench clinopyroxene (cpx) and the low Ca-number (0·71–0·78) of quench plagioclase (plag) in these samples. This observation suggests that the olivine crystals in these rocks are cumulate crystals that formed deep in a magma chamber at a high temperature before being brought to the surface by the eruption of more evolved melt with which the quench cpx and plag may be in closer equilibrium. The apparent zoning of the euhedral olivine crystals (Fig. 4) may suggest that their rims have lower Fo. However, it is not possible to examine the rims because of the alteration (Fig. 4). In any case, the cores of the olivine phenocrysts are likely to preserve the best record of the temperature of the parental melts (e.g. Nisbet *et al.*, 1993).

The average composition of the olivine phenocrysts is Fo = 0·902 ± 0·011 ($\pm 1\sigma$), which is close to the widely accepted mantle olivine composition (Dick, 1989; Herzberg & O'Hara, 1998, 2002; Griffin *et al.*, 1999). Assuming that the cores of the olivine phenocrysts are magmatic (versus xenocrystal), this points to very primitive parental melts having Mg-number = 0·73 ± 0·02 ($\pm 1\sigma$) by assuming $K_d = [X_{Mg}^{L}/X_{Fe}^{2+L})/[X_{Mg}^{ol}/X_{Fe}^{2+ol}] = 0{\cdot}3 \pm 0{\cdot}03$ (Roeder & Emslie, 1970). As the liquidus temperature is linearly related to the MgO content (not Mg-number) (e.g. Nisbet *et al.*, 1993) of the melt, precise determination of the liquidus temperatures of the melts parental to the observed olivine crystals in the picrite lavas is not straightforward. Following the experimental and theoretical work of Beattie *et al.* (1991), Nisbet *et al.* (1993) developed an empirical relationship between olivine Fo content and the MgO content in weight percent of the melt in equilibrium with the olivine. This $Fo^{ol}$–$MgO^{Melt}$ relationship, which can be described by a power-law equation of the form MgO (wt %) = 55 × $Fo^{11{\cdot}5}$ [derived from the work of Nisbet *et al.* (1993) assuming oxygen fugacity close to QFM (quartz–fayalite–magnetite)] is described by the curve in Fig. 5a. The Yunnan picrite whole-rock data, given their olivine Fo contents (from 0·889 to 0·919; Table 1), deviate far from the equilibrium curve towards very high MgO contents. This deviation corroborates the petrographic inference that the olivine crystals are of cumulate origin, formed at a high temperature deep in a magma chamber before eruption. Therefore, the temperature information contained in the olivine phenocrysts does not reflect eruption temperatures, but the temperatures at which the olivine crystallized from the parental melts with MgO contents indicated by the open arrows in Fig. 5a.

The MgO contents of the corresponding melts parental to the olivine crystals are also plotted in Fig. 5b. It should be noted that the calculated MgO contents of the parental melts vary significantly from ~14·1 wt % to ~20·8 wt %, and are sensitive to small changes in olivine Fo content. We can use these calculated MgO contents of the parental melts to estimate their liquidus temperatures, which again vary significantly from one sample to another, and also vary depending on the model (Fig. 5c). Using the low-pressure MgO–$T$ relationship of Nisbet (1982) and Renner (1989) for komatiites, and that of Niu *et al.* (2002*a*) for basalts based on high $P$–$T$ experimental data (see

*Table 2: Major and trace element compositions of Late Palaeozoic ultramafic and mafic pillow lavas in Yunnan, SW China*

| | Type I picrite | | | Type II picrite | | | Basalt |
|---|---|---|---|---|---|---|---|
| | YN14a | YN14b | YN16 | YN17 | MXE441 | MXE01 | YN18 |
| *wt %* | | | | | | | |
| $SiO_2$ | 41·03 | 42·00 | 42·45 | 41·69 | 41·97 | 39·74 | 52·55 |
| $TiO_2$ | 0·532 | 0·548 | 0·565 | 1·017 | 1·065 | 0·829 | 2·577 |
| $Al_2O_3$ | 7·479 | 7·817 | 8·793 | 5·596 | 5·378 | 4·139 | 13·14 |
| FeOt | 9·271 | 9·387 | 9·244 | 10·51 | 10·57 | 10·34 | 10·45 |
| MnO | 0·135 | 0·137 | 0·131 | 0·145 | 0·140 | 0·134 | 0·198 |
| MgO | 27·12 | 27·68 | 26·05 | 28·36 | 28·30 | 30·69 | 7·662 |
| CaO | 5·694 | 5·801 | 6·434 | 4·347 | 4·794 | 2·746 | 8·477 |
| $Na_2O$ | 0·693 | 0·673 | 0·690 | 0·130 | 0·149 | 0·108 | 3·272 |
| $K_2O$ | 0·032 | 0·038 | 0·050 | 0·074 | 0·115 | 0·062 | 0·772 |
| $P_2O_5$ | 0·062 | 0·059 | 0·051 | 0·155 | 0·194 | 0·177 | 0·498 |
| LOI (%) | 7·477 | 5·596 | 5·213 | 7·658 | 7·119 | 10·824 | 0·006 |
| Total | 99·53 | 99·74 | 99·68 | 99·67 | 99·79 | 99·79 | 99·61 |
| Mg-no. | 0·853 | 0·854 | 0·848 | 0·842 | 0·841 | 0·855 | 0·592 |
| $CaO/Al_2O_3$ | 0·761 | 0·742 | 0·732 | 0·777 | 0·892 | 0·663 | 0·645 |
| $Al_2O_3/TiO_2$ | 14·07 | 14·27 | 15·57 | 5·503 | 5·048 | 4·994 | 5·099 |
| *ppm* | | | | | | | |
| Li | 5·697 | 10·83 | 10·41 | 10·44 | 10·44 | 15·42 | 3·365 |
| Be | 0·118 | 0·125 | 0·122 | 0·361 | 0·285 | 0·236 | 0·672 |
| Sc | 21·80 | 21·52 | 21·07 | 13·99 | 13·83 | 11·28 | 23·06 |
| Ti | 3071 | 3019 | 3097 | 6055 | 5478 | 4137 | 9394 |
| V | 121·4 | 121·9 | 123·3 | 113·8 | 106·7 | 81·86 | 239·2 |
| Cr | 3135 | 2428 | 2262 | 2324 | 2191 | 2587 | 86·30 |
| Co | 92·97 | 93·06 | 90·49 | 96·20 | 95·84 | 103·3 | 36·31 |
| Ni | 1283 | 1203 | 1069 | 1558 | 1603 | 1815 | 135·8 |
| Cu | 83·58 | 73·00 | 72·30 | 54·41 | 61·09 | 44·30 | 102·4 |
| Zn | 66·14 | 59·30 | 58·02 | 89·08 | 85·13 | 88·07 | 103·2 |
| Ga | 8·196 | 8·054 | 8·637 | 7·471 | 7·406 | 6·773 | 15·70 |
| Rb | 1·721 | 1·892 | 2·624 | 10·94 | 13·21 | 6·011 | 7·076 |
| Sr | 59·20 | 58·02 | 79·55 | 62·55 | 69·55 | 38·94 | 254·1 |
| Y | 10·67 | 11·14 | 10·08 | 10·00 | 9·294 | 7·285 | 23·63 |
| Zr | 28·94 | 27·97 | 28·21 | 78·85 | 60·68 | 53·67 | 148·0 |
| Nb | 1·013 | 0·998 | 0·788 | 8·575 | 6·731 | 5·868 | 15·98 |
| Cs | 0·062 | 0·239 | 0·373 | 3·498 | 4·875 | 2·755 | 1·127 |
| Ba | 10·88 | 6·434 | 7·291 | 29·16 | 24·92 | 28·33 | 223·0 |
| La | 1·169 | 1·121 | 0·987 | 7·619 | 5·843 | 5·132 | 15·07 |
| Ce | 3·316 | 3·112 | 2·971 | 17·70 | 13·95 | 11·98 | 35·90 |
| Pr | 0·574 | 0·559 | 0·545 | 2·413 | 1·955 | 1·651 | 4·937 |
| Nd | 3·113 | 3·055 | 3·045 | 10·10 | 8·449 | 7·020 | 21·31 |
| Sm | 1·158 | 1·162 | 1·159 | 2·449 | 2·140 | 1·696 | 5·428 |
| Eu | 0·480 | 0·473 | 0·474 | 0·843 | 0·759 | 0·598 | 1·864 |
| Tb | 0·300 | 0·299 | 0·287 | 0·379 | 0·347 | 0·272 | 0·883 |
| Gd | 1·662 | 1·652 | 1·589 | 2·483 | 2·262 | 1·761 | 5·803 |
| Dy | 2·043 | 2·030 | 1·913 | 2·215 | 2·024 | 1·605 | 5·171 |
| Ho | 0·434 | 0·435 | 0·404 | 0·415 | 0·383 | 0·299 | 0·976 |
| Er | 1·250 | 1·254 | 1·146 | 1·073 | 1·000 | 0·781 | 2·526 |
| Tm | 0·185 | 0·181 | 0·167 | 0·143 | 0·135 | 0·105 | 0·336 |
| Yb | 1·147 | 1·140 | 1·046 | 0·849 | 0·804 | 0·614 | 1·987 |
| Lu | 0·175 | 0·177 | 0·161 | 0·121 | 0·116 | 0·088 | 0·282 |
| Hf | 0·857 | 0·816 | 0·829 | 2·034 | 1·659 | 1·427 | 3·925 |
| Ta | 0·053 | 0·051 | 0·042 | 0·515 | 0·415 | 0·363 | 0·970 |
| Pb | 0·382 | 0·359 | 0·301 | 0·589 | 0·715 | 0·488 | 0·487 |
| Th | 0·142 | 0·131 | 0·099 | 0·752 | 0·567 | 0·511 | 1·479 |
| U | 0·038 | 0·037 | 0·030 | 0·194 | 0·148 | 0·133 | 0·416 |
| Nb/Ta | 18·97 | 19·41 | 18·75 | 16·64 | 16·21 | 16·18 | 16·47 |
| Zr/Hf | 33·78 | 34·27 | 34·03 | 38·77 | 36·57 | 37·62 | 37·71 |
| Y/Ho | 24·61 | 25·62 | 24·97 | 24·09 | 24·28 | 24·40 | 24·22 |
| Th/U | 3·716 | 3·557 | 3·277 | 3·869 | 3·820 | 3·846 | 3·558 |
| Nb/U | 26·48 | 27·01 | 26·13 | 44·14 | 45·37 | 44·16 | 38·43 |
| Nb/Th | 7·13 | 7·59 | 7·97 | 11·41 | 11·88 | 11·48 | 10·80 |
| Ce/Pb | 8·684 | 8·678 | 9·882 | 30·05 | 19·53 | 24·55 | 73·73 |
| $[La/Sm]_{CN}$ | 0·652 | 0·623 | 0·549 | 2·009 | 1·762 | 1·953 | 1·792 |
| $[Sm/Yb]_{CN}$ | 1·122 | 1·133 | 1·232 | 3·204 | 2·960 | 3·071 | 3·035 |

Major element oxides determined by ICP-OES and trace elements determined by ICP-MS, at The University of Queensland. FeOt, total Fe expressed as FeO. Mg-number = $Mg/(Mg + Fe^{2+})$ assuming 10% total Fe as $Fe^{2+}$. The subscript CN stands for chondrite-normalized ratios.

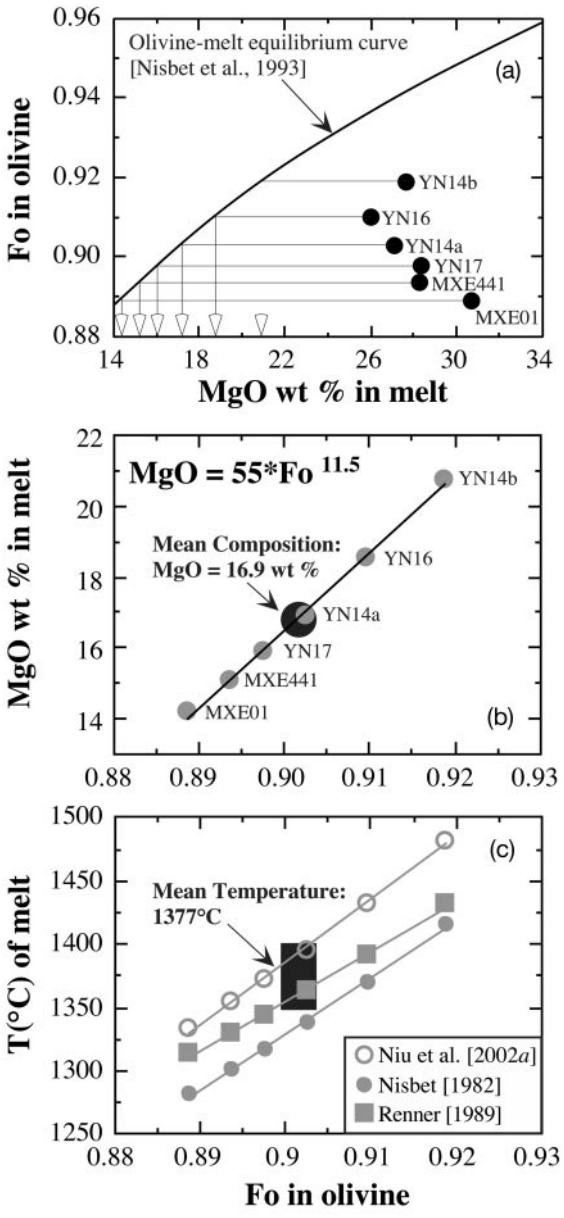


Fig. 5 caption for details), we can obtain a series of liquidus temperatures for the parental melts. Although the large variation in calculated MgO contents and liquidus temperatures could be real, the compound errors from the mineral compositional data to the model calculations may be large, and difficult to evaluate. For the purpose of discussion, we therefore, cautiously, use a mean MgO value of ~16·9 wt % to represent the parental magma composition, and a mean value of ~1377°C as the liquidus temperature for the parental melts in equilibrium with the olivine crystals observed in the Yunnan picrites.

Herzberg & O'Hara (2002) have recently developed a new technique that allows more precise estimation of liquidus temperatures of highly magnesian lavas from whole-rock compositions and olivine Fo contents (Fig. 6). Using this technique, the calculated primary magmas for the Yunnan picrites have a mean composition (corresponding to sample YN14a) of 18·6 wt % MgO, which is equivalent to a liquidus temperature of 1425°C (Herzberg & O'Hara, 2002). Both MgO content and liquidus temperature calculated this way are higher than conservative estimates based on empirical models (Fig. 5 and above). These results suggest that the Yunnan picrites are quite similar to the Cretaceous Gorgona komatiites (Fig. 6) (e.g. Kerr *et al.*, 1996; Arndt *et al.*, 1997; Herzberg & O'Hara, 1998, 2002; Révillon *et al.*, 2000), and are thus consistent with a mantle plume origin. We also noted the report that melt inclusions in spinifex-textured olivine from the Gorgona komatiites have a lower MgO content of 14·29 ± 0·71 wt % (Sylvester *et al.*, 2000).

The inferred MgO content (~17–19 wt %; see above) of the primary magmas for the Yunnan picrites is unusually high for mantle-derived magmas in any present-day tectonic setting. The inferred liquidus temperature (~1377–1425°C or 1400 ± 25°C) is higher than would be expected in the present-day mantle given a postulated present-day mantle potential temperature of 1280°C (McKenzie & Bickle, 1988) or 1350°C as we prefer (see Fig. 7 caption for details) derived from mid-ocean ridge basalts (MORB). Figure 7 shows the probable mantle potential temperature of 1540 ± 30°C for the petrogenesis of the Yunnan picrites. This latter temperature is even higher than model secular cooling curves for the upper mantle as suggested by Richter (1988) and others

**Fig. 5.** (a) An empirical curve (MgO = 55 × $Fo^{11·5}$) representing the equilibrium relationship between olivine forsterite content and MgO wt % in the melt. This curve is derived from the work of Nisbet *et al.* (1993), who used experimental data in the literature. Plotting of Yunnan ultramafic lavas using olivine Fo contents and whole-rock MgO indicates that the lavas are not true melt compositions, but possess excess cumulate olivine crystals. The MgO contents of the melt in equilibrium with the constituent olivine are indicated by the open arrows. (b) MgO contents of parental melts in equilibrium with olivine crystals calculated using curve in (a) are plotted. A mean value of 16·9 wt % MgO is indicated by the large black circle. (c) Liquidus temperatures calculated from MgO in (b) using different models: Nisbet (1982) and Renner (1989) for komatiites, and Niu *et al.* (2002*a*) based on many experimental and theoretical studies for basalts (e.g. Roeder & Emslie, 1970; Bender *et al.*, 1978; Walker *et al.*, 1979; Langmuir & Hanson, 1981; Nielsen & Dungan, 1983; Weaver & Langmuir, 1990; Grove *et al.*, 1992): (i) $T_{liquidus}(°C) = 1026e^{[0·01894MgO(wt\ \%)]}$ or (ii) $T_{liquidus}(°C) = 1066 + 12·067$ Mg-number $+ 312·3$(Mg-number)$^2$, where Mg-number = Mg/(Mg + Fe) of the equilibrium melt. The liquidus temperature of olivine is derived from (ii) with Mg-number calculated from olivine using: Mg-number(melt) = $1/\{[1/(Fo - 1)]/K_d + 1\}$, where $K_d = 0·30 \pm 0·03$ (Roeder & Emslie, 1970). Given the large variations in calculated liquidus temperatures within the sample suites and between models, and model uncertainties, a mean value of 1377°C is indicated within the black rectangle.

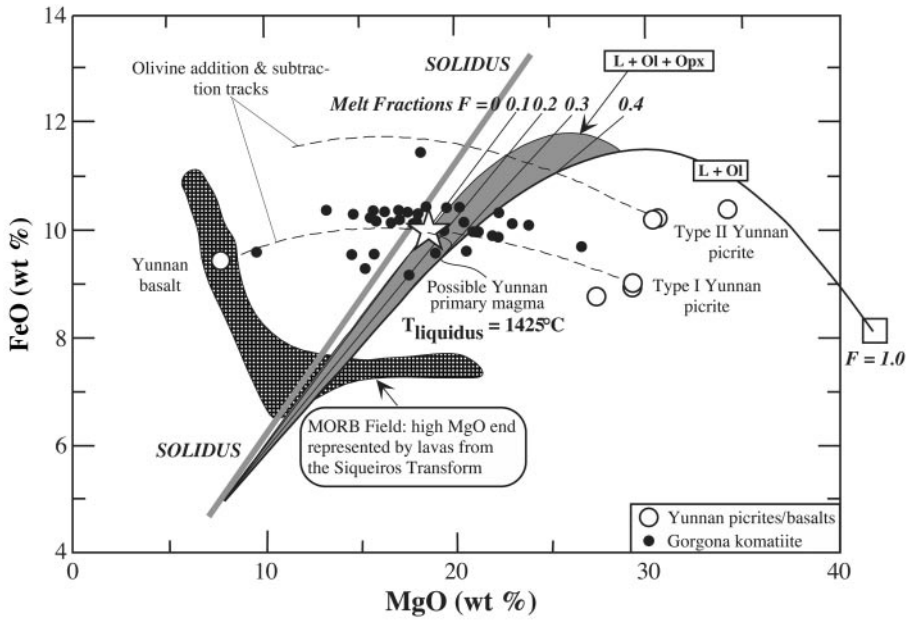


**Fig. 6.** The Yunnan picrites and basalt plotted in FeO–MgO space to compare with MORB and the Gorgona komatiites along with models of accumulated fractional melting from a depleted MORB mantle by Herzberg & O'Hara (2002). This model is superior to all existing models (e.g. see Fig. 5) in that this new model uses a much larger experimental database spanning a greater pressure range and involves interfacing phase equilibrium projections using absolute weight percentage of FeO and MgO for both equilibrium and fractional melting. This model gives a possible primary magma of 18·6 wt % MgO and 10·0 wt % FeO parental to the Yunnan picrites, yielding a liquidus temperature of 1425°C. This comparison suggests that the parental magma composition and melting conditions of the Yunnan picrites resemble those of Gorgona komatiites (Herzberg & O'Hara, 2002). This figure is slightly modified from that kindly provided by Claude Herzberg.

for the Late Palaeozoic. We therefore infer from these calculations that the Yunnan picrites are genetically associated with deep mantle melting, and are probably products of mantle plumes or hotspots in Late Palaeozoic time. The field lithological association further suggests that the Yunnan picrites may represent an ocean island or oceanic plateau setting (e.g. Fang *et al.*, 1996). We note that Green *et al.* (2001) have suggested a present-day mantle potential temperature of 1430°C that is the same beneath ocean ridges and ocean islands.

## Major and trace element data favour a mantle plume origin

The Yunnan picrite lavas have two compositionally distinct groups (Table 2 and Figs 8 and 9) that correspond to the two rock types identified petrographically: Type I picrites (YN14a, YN14b and YN16) are depleted in incompatible elements, whereas Type II picrites (YN17, MXE441 and MXE01) are enriched in incompatible elements. Panels in rows (a) and (b) of Fig. 8 show that the major elements are decoupled from the incompatible trace elements, but coupled with the compatible trace elements. This suggests that Type I and Type II picrites have different parental melts with different incompatible element abundances in the first place (e.g. the inverse $Na_2O$–La and FeO–$Na_2O$ trends), and also reflects the fact that the compositions of the lavas do not represent true liquid composition, but contain cumulate minerals. As a result, cumulate olivine (plus some minor cumulate cpx) and quenched groundmass (quench cpx and plag and devitrified glass altered to chlorite, tremolite, etc.) determine the bulk-rock major element compositions. For example, the positive $Na_2O$–$Al_2O_3$–CaO correlations indicate that the parental magmas for Type I picrites (vs Type II) are enriched in these elements as reflected by the presence of quench plagioclase, which is absent in enriched Type II picrites. It should be noted that the significant inverse trends of $Al_2O_3$–Ni and CaO–Co result from differences in both parental melt compositions and modal mineralogy. Row (c) in Fig. 8 shows that the between-type distinctions also apply to mobile incompatible elements (alkalis such as K, Rb and Cs plus Pb). These scattered, yet significant, positive trends between moderately incompatible–immobile elements such as $TiO_2$ and highly incompatible and mobile elements suggest that the post-magmatic alteration has not entirely erased the primary igneous signatures of these otherwise mobile elements (except for Sr, which is uncorrelated with any element of interest).

It is important to note the nearly perfect correlations [rows (d) and (e) of Fig. 8] between incompatible and

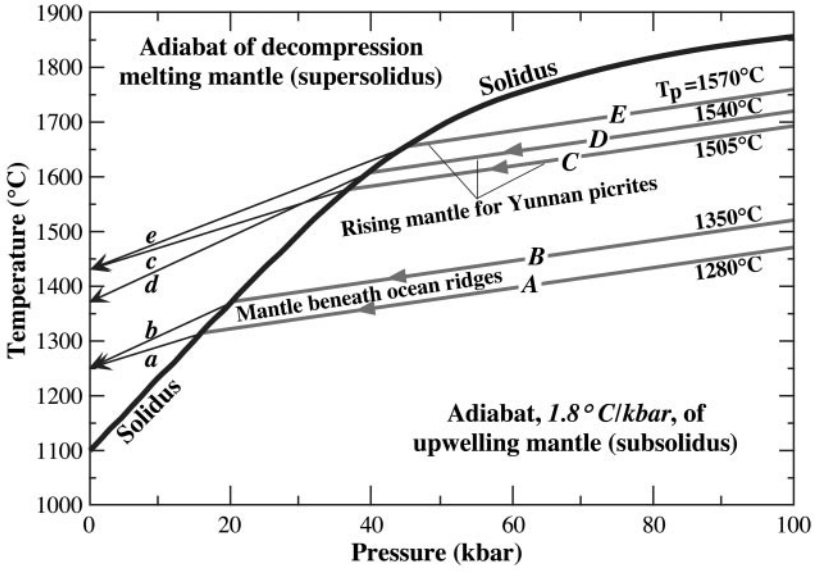


**Fig. 7.** Estimation of potential temperatures of the upwelling mantle that produced the Yunnan picrites in $P$–$T$ space. The solidus is taken from McKenzie & Bickle (1988) and is based on averaged experimental data. Mantle potential temperature ($T_p$) is defined as the temperature that a solid parcel of mantle would have if brought to the surface along an adiabatic thermal gradient (McKenzie & Bickle, 1988). Estimation of mantle potential temperature from the erupted lavas requires knowledge of (1) the mantle adiabat under subsolidus conditions $[(\partial T / \partial P)_{Adiabat}^{Solid\text{–}M}]$, (2) the adiabat of the decompression-induced melting mantle $[(\partial T / \partial P)_{Adiabat}^{Molten\text{–}M}]$, and (3) liquidus temperatures ($T_{liquidus}$) of primary magmas extracted from the melting mantle without experiencing shallow-level cooling. There is good agreement on $[(\partial T / \partial P)_{Adiabat}^{Solid\text{–}M}] \sim 1{\cdot}8$°C/kbar (e.g. McKenzie & Bickle, 1988; Langmuir *et al.*, 1992; Asimow *et al.*, 2001; Herzberg & O'Hara, 2002). The $[(\partial T / \partial P)_{Adiabat}^{Molten\text{–}M}]$ is, however, not well constrained, varying between 4 and 6°C/kbar (e.g. McKenzie & Bickle, 1988; Langmuir *et al.*, 1992; Asimow *et al.*, 2001; Herzberg & O'Hara, 2002). To evaluate the $T_{liquidus}$ of primary magmas requires an understanding of the cooling history of magmas before their eruption, which is not straightforward. The recent comprehensive model by Herzberg & O'Hara (2002) represents the best effort in this regard, in particular for high-magnesian lavas derived from mantle plumes. The $T_p$ for MORB mantle has been used widely as a reference point. The primary MORB melts are likely to have 11–13 wt % MgO (Niu & Batiza, 1991; Niu, 1997), but as the most primitive MORB melts have <10·5 wt % MgO (e.g. Hékinian *et al.*, 1995), the minimum MORB mantle $T_p$ can be estimated by assuming a primary melt of 10·5 wt % MgO, which is equivalent to $T_{liquidus} \sim 1250$°C. Assuming $[(\partial T / \partial P)_{Adiabat}^{Molten\text{–}M}] = 4$°C/kbar, $T_p \sim 1280$°C (curves *a* and *A*) (McKenzie & Bickle, 1988). This would imply that the rising MORB mantle begins to melt at pressures <20 kbar, which is inconsistent with petrological observations (e.g. Klein & Langmuir, 1987; Niu & Batiza, 1991; Niu, 1997). If $[(\partial T / \partial P)_{Adiabat}^{Molten\text{–}M}] = 6$°C/kbar is considered, $T_p \sim 1350$°C (curves *b* and *B*) (Niu *et al.*, 2001). This is more consistent with the petrological observations, although $T_p \sim 1350$°C is likely to be the minimum (see above). For the Yunnan picrites, if we used $T_{liquidus} \sim 1377$°C (Fig. 5), and $[(\partial T / \partial P)_{Adiabat}^{Molten\text{–}M}] = 6$°C/kbar, then $T_p \sim 1540$°C (curves *d* and *D*). Assuming $T_{liquidus} \sim 1425$°C (Fig. 6), and $[(\partial T / \partial P)_{Adiabat}^{Molten\text{–}M}] = 4$°C/kbar, then $T_p \sim 1505$°C (curves *c* and *C*). If $[(\partial T / \partial P)_{Adiabat}^{Molten\text{–}M}] = 5$°C/kbar is used, $T_p \sim 1570$°C (curves *e* and *E*). It should be noted that $[(\partial T / \partial P)_{Adiabat}^{Molten\text{–}M}] = 6$°C/kbar would be erroneous in this case as the upwelling mantle would not intersect the solidus, which reflects the likely uncertainty in all relevant parameters, including probable errors associated with the solidus. In any case, $T_p \sim 1540 \pm 30$°C is reasonable for the genesis of the Yunnan picrites, which is ~200°C hotter than for MORB genesis, $T_p \sim 1350$°C.

highly incompatible elements (e.g. La, Ce, Zr, Hf, Nb, Ta, Th, U) in the Yunnan picrites. (Note the similar abundances in depleted Type I lavas, but variable abundances in enriched Type II lavas for a given element.) Given the fact that these lavas are rather altered and U would be fairly mobile during post-magmatic alteration under oxidizing conditions (i.e. in the form of $U^{6+}$), the systematic co-variation of U with all these immobile (e.g. La, Ce, Th, etc.) and highly immobile (Nb, Ta, Zr, Hf, etc.) elements demonstrates unequivocally that U was not mobile during the alteration. This suggests that elemental ratios involving U and other immobile elements in these rocks reflect primary igneous signatures. This is important because ratios such as Th/U, Nb/U and Nb/Th in mafic or ultramafic lavas have been widely used not only to identify the tectonic settings in which the melts may have formed (e.g. Hofmann, 1988; Sun & McDonough, 1989; McDonough & Ireland, 1993; Pearce & Peate, 1995), but also to infer the nature and time scales of the Earth's chemical differentiation and continental crust accretion (e.g. Hofmann, 1988; Niu & Batiza, 1997; Sylvester *et al.*, 1997; Collerson & Kamber, 1999; Niu *et al.*, 1999, 2002*b*; Campbell, 2001).

Table 2 shows that both depleted (Type I) and enriched (Type II) Yunnan picrites together with a basalt from the Type II picrite site define a narrow range of Th/U = 3·62 ± 0·23, which is almost identical to chondritic ratio of 3·625, slightly lower than that of average ocean island basalts (OIB; ~3·92), primitive mantle (~4·00), and continental crust (~3·94), but significantly greater

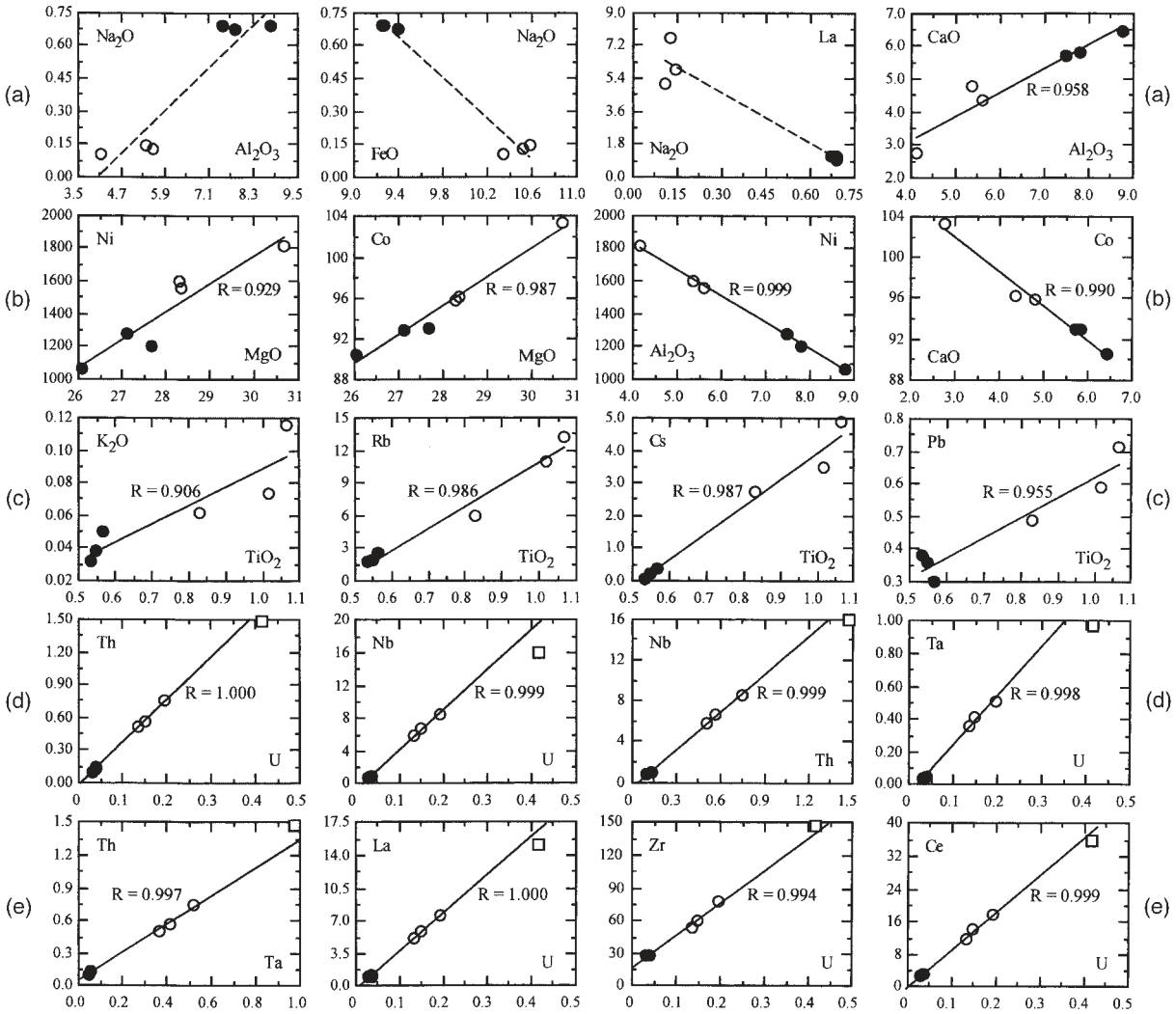


**Fig. 8.** Binary element–element plots for the Yunnan ultramafic lavas. ●, Type I depleted picrites (YN14a, YN14b and YN16); ○, Type II enriched picrites (YN17, MXE441 and MXE01); □, alkali basalt (YN18) from Type II picrite site. Row (a) shows the good separation between the two types in both major and incompatible trace elements. The high $Na_2O$, $Al_2O_3$ and CaO in depleted Type I picrite are mostly controlled by the parental melts that are enriched in these elements as reflected by the quench microlites of plagioclase in these samples, which do not exist in Type II picrite. Row (b) also shows the distinction between the two types of lavas. Row (c) shows the scattered yet significant correlations between immobile–moderately incompatible $TiO_2$ and mobile and highly incompatible elements, which is unexpected for these highly altered lavas (note the up to 10% LOI in some samples). Rows (d) and (e) show almost perfect correlations among several important elements. It should be noted that the regression lines are derived from picrite lavas only, and the basalt (YN18) is plotted only for comparison.

than average mid-ocean ridge basalts (MORB; ~2–3), and island arc basalts (IAB; variable, but mostly <2 in arcs with limited terrigenous sediment input) (e.g. Hofmann, 1988; Sun & McDonough, 1989; Rudnick & Fountain, 1995; Niu & Batiza, 1997; Ewart *et al.*, 1998; Niu *et al.*, 1999; Y. Niu, unpublished data, 2002). The Th/U ratios alone suggest that the Yunnan picrites are of mantle plume origin. Although it may be argued that the elevated Th/U ratios could be due to continental crust assimilation, this argument is unsupported by other ratios, major element data, and the fact that the Th/U ratio is the same for both depleted and enriched lavas.

The distinctive between-type, but constant within-type Nb/U ratios (~26·5 for depleted Type I picrites; ~44·6 for enriched Type II picrites; 38·4 for the basalt) overlap MORB data (Niu & Batiza, 1997), but differ from average MORB and OIB (~40–50) (Hofmann, 1988; Sun & McDonough, 1989), and are significantly greater than that of IAB, which is variable but mostly <10 (Ewart *et al.*, 1998; Y. Niu, unpublished data, 2002). It should be noted that Nb/U ~26·5 in Type I depleted picrites is lower than chondritic and primitive mantle ratios (~30–34). The distinctive between-type, but constant within-type Nb/Th ratios (~7·56 for depleted Type I

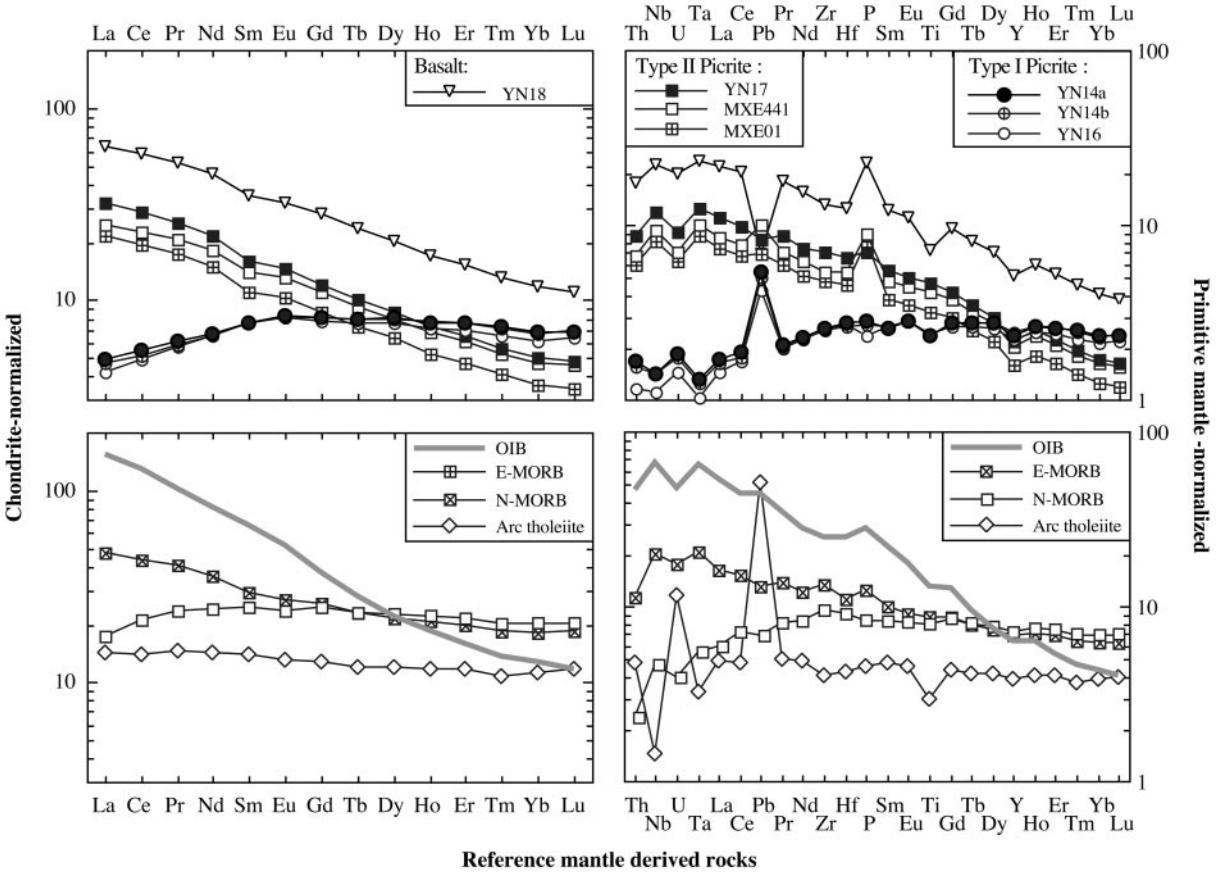


**Fig. 9.** Chondrite-normalized REE patterns of the Yunnan picrite and basalt lavas on the left and primitive mantle normalized trace element variation diagrams on the right. Average compositions of mantle-derived rocks are plotted in the bottom two panels for comparison. Chondritic and primitive mantle values, and average OIB compositions are from Sun & McDonough (1989). N- and E-MORB values are averages of high-quality ICP-MS analyses of MORB and East Pacific Rise near-ridge seamount samples from Niu & Batiza (1997) and Niu *et al.* (2002*b*). Arc tholeiites are average values of Ewart *et al.* (1998) and unpublished data (Y. Niu, 2002) for Tonga and Mariana arcs. It should be noted that the apparent positive Pb anomalies of the Type I picrites are real features.

picrites; ~11·6 for enriched Type II picrites; 10·8 for the basalt) are lower than MORB ratios (>14), but significantly greater than those of the continental crust and IAB (<4). In fact, the enriched Type II picrites and the basalt have Nb/Th ratios that are very close to the average OIB value of ~12 (Sun & McDonough, 1989), and similar to many lavas from the Ontong Java plateau (Campbell, 1998). It should be noted that the depleted Type I picrites have Nb/Th ratios (~7·56) that are very close to chondritic or primitive mantle values (Hofmann, 1988; Sun & McDonough, 1989).

The foregoing discussion and the detailed comparisons of the Yunnan picrites and basalt with average mantle-derived rocks in Fig. 9 (bottom panels) allow us to conclude that these rocks differ significantly from MORB, IAB and continental crust. We are thus left with the possibility that these lavas are indeed genetically associated with mantle plumes or hotspots. The variations of Nb/Th and Nb/U within these lavas with respect to 'typical' plume materials and the fact that mantle plume sources can both be enriched (e.g. $[La/Sm]_N > 1$) and depleted (e.g. $[La/Sm]_N < 1$) indeed reflect compositional heterogeneities in plume sources as expected in terms of mantle plume dynamics and as observed in plume products (e.g. Arndt *et al.*, 1997; Fitton *et al.*, 1997; Campbell, 1998). It is necessary to note that the Th/U ratio in both types of the Yunnan picrites, and the Nb/Th and Nb/U ratios in the depleted Type I Yunnan picrites resemble, to some extent, chondritic values or values of the primitive mantle (e.g. Sun & McDonough, 1989). This could be interpreted as resulting from an 'undifferentiated' primitive mantle reservoir in the lower mantle. This interpretation, however, cannot be correct because melts derived from an undifferentiated primitive mantle cannot produce incompatible element depleted Type I Yunnan picrites. The latter can only be derived from a source that had already been depleted in incompatible elements in the past (e.g. previous melt extraction). The geo-

chemical data of the depleted Type I Yunnan picrites in fact contribute to our understanding of the nature of the depleted mantle in the Late Palaeozoic.

## 'Were komatiites wet'?

The resemblance of the Yunnan picrites to the Cretaceous komatiites on Gorgona Island (see above) suggests that the Yunnan picrite data may contribute to the komatiite debate—whether the high-MgO Archaean komatiites resulted from hydrous melting at low temperatures in a convergent-margin setting (e.g. Parman *et al.*, 1997; Stone *et al.*, 1997; Grove *et al.*, 1999) or anhydrous melting at very high temperatures associated with mantle plumes (e.g. Bickle, 1993; McDonough & Ireland, 1993; Nisbet *et al.*, 1993; Arndt *et al.*, 1998; Herzberg & O'Hara, 1998; Herzberg, 1999). Indeed, komatiite melts, at least some, must not be entirely dry as evidenced by the presence of some primary hydrous phases and primary vesicles (e.g. Stone *et al.*, 1997). Primary vesicles are relatively abundant in the Yunnan picrites. Assuming komatiites were formed by high-degree melting of hydrous mantle at lower temperatures and shallower depths (e.g. Grove *et al.*, 1999), then the first pertinent question is where in the global tectonic framework hydrous mantle may exist. The likely setting would be the mantle wedge above subduction zones where the mantle may become hydrous as the result of subducting slab dehydration. This is indeed the very environment in which the 'wet komatiites' were proposed to have originated by Allègre (1982), and more recently by Grove *et al.* (1999) based on their experimental studies on the Barberton komatiites, the oldest (~3·49 Ga), and thought to be the hottest komatiite melts with highest MgO (up to 33 wt %) (e.g. Nisbet *et al.*, 1993). This hydrous melting model assumes without elaboration that plate tectonics were already in operation 3·5 Gyr ago, which is not unlikely, but requires observational evidence. The hydrous melting model would also suggest that komatiites should have geochemical systematics that resemble IAB, i.e. enrichments in incompatible–mobile elements such as K, Rb, Cs, Sr, Pb, U, etc. relative to incompatible–immobile elements such as Nb, Ta, Zr, Hf and, to a lesser extent, Th, and light REE such as La, Ce, Pr, etc. These characteristics are not observed in komatiite melt inclusions (e.g. McDonough & Ireland, 1993). The geochemical signatures of Nb–Th–U in the Yunnan picrites discussed above (also see details in Fig. 9) do not in any way resemble IAB, but instead favour a mantle plume origin. It may be argued that in the Archaean U may behave as an immobile element as $U^{4+}$ during slab-dehydration reactions and mantle wedge melting because of the prevailing oxygen-poor atmosphere and hydrosphere (e.g. Sylvester *et al.*, 1997; Collerson & Kamber, 1999), thus giving no U enrichments in the komatiite melts. However, the geochemical behaviour of Th (4+) is independent of oxygen fugacity, and we would expect Nb/Th <4, Nb/U <10 and Th/U <2 in all Archaean komatiites as in present-day IAB, but this is not observed. If the Yunnan Late Palaeozoic picrites can be considered as a Phanerozoic analogy to Archaean komatiites, then these young 'komatiites' do not appear to be related in any manner to suprasubduction-zone hydrous mantle melting. In conclusion, komatiites may not be entirely dry, but they are not formed in mantle wedges above subduction zones. At least for the Yunnan picrites (or komatiites), the available data are most consistent with a mantle plume origin.

## Some remarks on the use and implication of Th/U, Nb/Th and Nb/U

Th/U, Nb/U and Nb/Th ratios in mantle-derived rocks have been used to infer the nature and time scales of the Earth's chemical differentiation and continental crust accretion (e.g. Hofmann, 1988; Sylvester *et al.*, 1997; Collerson & Kamber, 1999; Campbell, 2001). Given the possible mobility of U during post-magmatic alteration under oxidizing conditions, U has been considered an unreliable element and some workers have used Th as a proxy for U (e.g. Johum *et al.*, 1991). The discovery of the immobility of U in altered 2·7 Ga komatiites and basalts by Sylvester *et al.* (1997) suggests, however, that fairly reduced conditions may have existed by this time, reaffirming the usefulness of U. Taking a step forward, Collerson & Kamber (1999) constructed Th/U, Nb/U and Nb/Th variation curves using their selected data from the literature on komatiites, basalts, gabbros and tonalites as a function of time from ~3·8 Ga to the present as shown by the bold lines in Fig. 10. By assuming that all these selected basaltic and komatiitic rocks were derived from the depleted mantle, these workers interpreted these curves in terms of the evolution of the Earth's atmosphere and continental crustal growth. For example, the steep increase in Nb/Th and Nb/U from 3·0 Ga to 2·0 Ga was interpreted as resulting from more effective removal of Th and U (vs Nb) from the mantle to the continental crust through subduction-zone processes by implicitly assuming that continental crust accretion is purely through subduction-zone magma genesis. The continuous increase in Nb/Th from 2·0 Ga onward was interpreted similarly, but at a slower rate. However, the decrease of Nb/U from 2·0 Ga onward was interpreted to result from a sudden elevation of free oxygen in the atmosphere, which created a more oxidizing global environment, causing U to behave as $U^{6+}$, which is soluble in aqueous solutions, in rivers, and

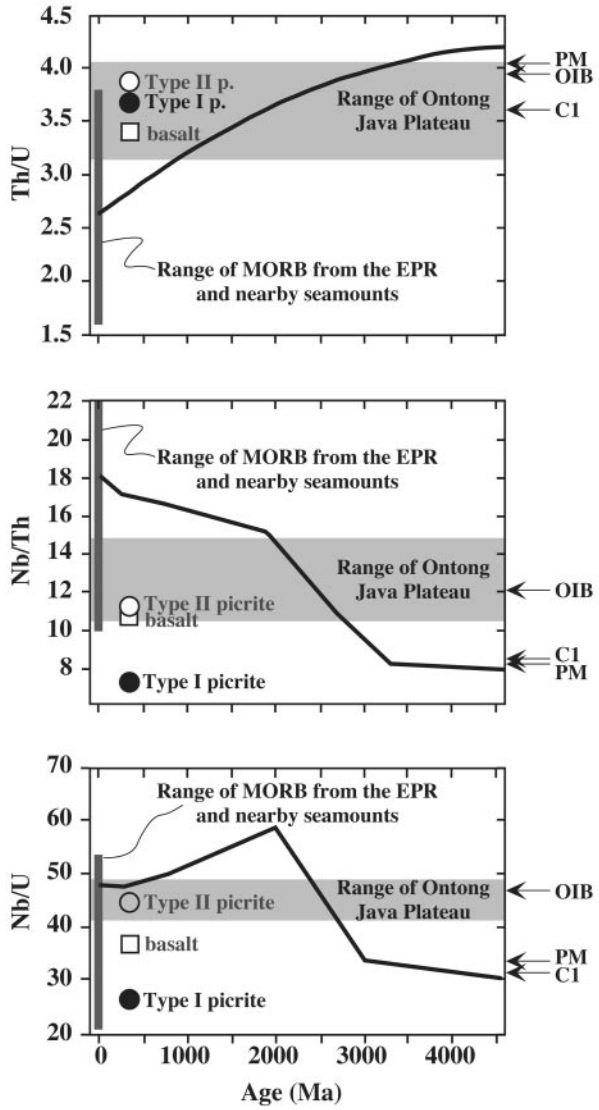


**Fig. 10.** Secular variation curves of Th/U, Nb/Th and Nb/U inferred to reflect the evolution of the depleted mantle constructed by Collerson & Kamber (1999) using their selected data from the literature on komatiites, basalts (including arc basalts), gabbros and tonalites. The Late Palaeozoic (assuming ~300 Ma) picrites and basalt from Yunnan, SW China, are plotted for comparison. Also plotted for comparison are high-quality data on MORB from the East Pacific Rise (EPR) axis and nearby seamounts (Niu & Batiza, 1997; Niu *et al.*, 1999, 2002*b*; Regelous *et al.*, 1999), the range of basalts from Malaita Island on the Ontong Java Plateau (Campbell, 1998), and average compositions of ocean island basalts (OIB), carbonaceous chondrite (C1) and primitive mantle (PM) of Sun & McDonough (1989). The significant departure of all the data from the Collerson & Kamber curves should be noted, in particular, the depleted Type I picrites, which should reflect the depleted mantle composition. Undoubtedly, inclusion of these depleted picrite data, and perhaps many other data of good quality will lead to significant revision of the secular curves, which will result in new interpretations. It should be noted that U in the Yunnan picrites and basalt is shown to be immobile, and thus that the Th/U, Nb/Th and Nb/U ratios in these rocks are reliable geochemical parameters.

in the oceans. As a result, progressively more U was returned into the depleted mantle in the form of hydrous phases carried by subducting oceanic crust. Although this interpretation is interesting, it neglects the fact that $U^{6+}$ would be more mobile and more effectively transported to the continents via subduction-zone magma genesis. As a result less U would be returned to the depleted mantle. This latter argument is substantiated by the fact that average present-day IAB have Th/U <2 in arcs with limited terrigenous sediment input, and have Nb/U <10, suggesting that U is more effectively transported into the continents (vs Th and Nb) rather than recycled into the depleted mantle. Th/U and Nb/U ratios in IAB are lower than the documented ratios of any of the present-day mantle reservoirs, including the depleted MORB mantle. It should be noted that Collerson & Kamber (1999) chose E-type, not N-type MORB for the present-day MORB mantle. On this basis, both Th/U and Nb/U ratios should increase, not decrease, in the depleted mantle as opposed to the declining curves in Fig. 10 since 2·0 Ga. There are two possibilities: (1) the secular variation curves of Collerson & Kamber (1999) are incorrect and more high-quality data on mafic and ultramafic rocks derived from the depleted mantle are needed to reconstruct the secular variation curves; (2) processes other than those proposed by Collerson & Kamber may have been operative in the last 2·0 Gyr.

Importantly, the apparent immobility of U in the altered Late Palaeozoic Yunnan picrites challenges the assumption that U has become mobile since 2·0 Ga owing to the change from an anoxic to a free oxygen-bearing atmosphere since 2·0 Ga. It is possible that the alteration of the Yunnan picrites may have taken place in a locally reduced environment, but the preservation of primary vesicles, intercalated cherts, and limestones altogether suggest that the alteration may have taken place in a system open to near-surface conditions. As discussed and concluded above and shown in Table 2 and Figs 8 and 9, the Yunnan picrites are of plume origin from a heterogeneous mantle source. The Type II picrites and the basalt are enriched in incompatible elements, but Type I picrites are depleted. We thus can assume that the depleted Type I picrite source may represent some portion of the depleted mantle entrained by the rising plume. Plotting the picrite data, in particular the depleted Type I data, onto the Collerson & Kamber plot in Fig. 10 reveals significant departures from the Collerson & Kamber curves in the Late Palaeozoic (~300 Ma assumed). This departure and the fact that we see from the altered Yunnan picrites no U mobility enforce the above suggestion that the secular variation of Th/U, Nb/Th and Nb/U in the depleted mantle must be reconstructed using high-quality data on samples that

truly reflect depleted mantle. Therefore, interpretations based on the existing curves must be reconsidered.

## SUMMARY

(1) The ultramafic lavas (MgO >26 wt %) in the Late Palaeozoic marine sequences in Yunnan, SW China, represent an extremely rare case in the Phanerozoic, second to the Cretaceous Gorgona komatiites. Given the lack of the spinifex-textured olivine in the Yunnan ultramafic lavas, we prefer to term them high-magnesian picrites, not komatiites.

(2) Although the Yunnan picrites possess cumulate olivine, which leads to high bulk-rock MgO contents, the presence of phenocrystal olivine with Fo = 0·902 ± 0·011 suggests that their parental melts may have had MgO of 17–19 wt %, similar to those inferred from the spinifex-textured Gorgona komatiites. This suggests that the liquidus temperature of the primary magmas parental to the Yunnan picrites was about 1400 ± 25°C. Such liquidus temperatures imply a mantle potential temperature of ~1540 ± 30°C, which is inconsistent with melting beneath mid-ocean ridges or in the mantle wedge above a subduction zone, but is consistent with a mantle plume origin. Their occurrence within the marine sequences suggests that the Yunnan picrites and associated basalts are best interpreted as components of an oceanic plateau developed in the Tethys ocean basin in the Late Palaeozoic. Trace element geochemical data for both the picrites and the basalt are consistent with a mantle plume origin.

(3) If the Yunnan picrites can be considered as a Phanerozoic analogy to the Archaean komatiites, the petrological and geochemical data for the Yunnan picrites would suggest that komatiites may not be entirely dry, but the lack of geochemical characteristics typical of island arc basalts does not support models of komatiite formation by hydrous mantle melting in the mantle wedge above subduction zones.

(4) The Yunnan picrites studied fall into two distinct groups in terms of both petrography and bulk-rock major and trace element geochemistry. Type II picrites and the basalt are enriched in incompatible elements with $[La/Sm]_N > 1$, whereas Type I picrites are depleted in incompatible elements with $[La/Sm]_N < 1$, suggesting a compositionally heterogeneous plume source.

(5) Although all of the Yunnan picrites studied are altered with the glassy matrix devitrified and replaced by secondary chlorite, tremolite and other phases, U abundances vary coherently with other immobile and incompatible elements such as Nb, Ta, Zr, Hf, La and Ce. This demonstrates that U was immobile or unaffected by the alteration processes and preserves a primary igneous signature. This further suggests a fairly reduced condition of alteration, either locally or perhaps reflecting the typical situation in the Late Palaeozoic. The latter inference requires serious consideration because the results, whatever they may be, are of global tectonic significance.

(6) The Th/U, Nb/Th and Nb/U ratios in these altered picrites can be used to infer the involvement of a mantle plume source in the Late Palaeozoic. The incompatible element depleted Type I picrites should provide some relevant information on the Th/U, Nb/Th and Nb/U ratios of depleted mantle component at that time. The significant departure of these ratios in depleted Type I picrites from those secular curves constructed using selected data in the literature requires (a) revision of the curves with better quality data on samples truly representing the depleted mantle throughout the Earth's history, and (b) reconsideration of the interpretations of the evolution of the Earth's atmosphere and the inferred continental growth model based on those curves.

(7) Finally, we hope to draw the attention of the international community to the Yunnan ultramafic lavas for more comprehensive research. Detailed geochronological and regional tectonic studies are urgently required to place temporal and spatial constraints on proposed mantle plume activity in the context of the global tectonic evolution in the Late Palaeozoic.

## ACKNOWLEDGEMENTS

We acknowledge assistance in the field and discussion with Qi Zhang, Qing Qian, Sun-ling Chung, Qin-hua Luo and Tong-yi Li; N.F. acknowledges support from Chinese NSF grant 49172102. Y.N. thanks the Australian Research Council for support of the field and analytical work carried out during his tenure at The University of Queensland. Y.N. also acknowledges the full support of UK NERC for a Senior Research Fellowship. We also thank Robert Cirocco and Alan Greig for analytical assistance, and Claude Herzberg for making projections and calculating the compositions of primary magmas for Yunnan picrites. Discussion with Mike O'Hara has always been helpful. Andy Saunders, Balz Kamber and Claude Herzberg are thanked for their constructive comments on an early version of the manuscript. Patience, constructive comments and great editorial effort by Marjorie Wilson and Alastair Lumsden have improved the paper significantly, for which we are grateful.

## REFERENCES

Allègre, C. A. (1982). Genesis of Archean komatiites in a wet ultramafic subducted plate. In: Arndt, N. T. & Nisbet, E. G. (eds) *Komatiites*. London: George Allen & Unwin, pp. 495–500.

Arndt, N. T. & Nisbet, E. G. (1982). What is a komatiite? In: Arndt, N. T. & Nisbet, E. G. (eds) *Komatiites*. London: George Allen & Unwin, pp. 19–22.

Arndt, N. T., Kerr, A. C. & Tarney, J. (1997). Dynamic melting in plume heads: the formation of Gorgona komatiites and basalts. *Earth and Planetary Science Letters* **146**, 289–301.

Arndt, N. T., Ginibre, C., Chauvel, C., Albarède, F., Cheadle, M., Herzberg, C., Jenner, C. & Lahaye, Y. (1998). Were komatiites wet? *Geology* **26**, 739–742.

Asimow, P. D., Hirschmann, M. M. & Stolper, E. M. (2001). Calculation of peridotite partial melting from thermodynamic models of minerals and melts, IV. Adiabatic decompression and the composition and mean properties of mid-ocean ridge basalts. *Journal of Petrology* **42**, 963–998.

Beattie, P., Ford, C. & Russell, D. (1991). Partition coefficients for olivine–melt and orthopyroxene–melt systems. *Contributions to Mineralogy and Petrology* **109**, 212–224.

Bender, J. F., Hodges, F. N. & Bence, A. E. (1978). Petrogenesis of basalts from the project FAMOUS area: experimental study from 0 to 15 Kbars. *Earth and Planetary Science Letters* **25**, 213–254.

Bickle, M. (1993). Plume origin for komatiites. *Nature* **365**, 390–391.

Campbell, I. H. (1998). The mantle's chemical signature: insights from the melting products of mantle plume. In: Jackson, I. (ed.) *The Earth's Mantle: Composition, Structure and Evolution*. Cambridge: Cambridge University Press, pp. 259–310.

Campbell, I. H. (2001). Implications of Nb/U, Th/U and Sm/Nd variations in plume magmas for the relationship between continental and oceanic crust formation and the development of the depleted mantle. In: *EUG 11 Abstract Volume*. Cambridge: Cambridge Publications, p. 428.

Collerson, K. D. & Kamber, B. S. (1999). Evolution of the continents and the atmosphere inferred from Th–U–Nb systematics of the depleted mantle. *Science* **283**, 1519–1552.

Dick, H. J. B. (1989). Abyssal peridotites, very slow spreading ridges and ocean ridge magmatism. In: Saunders, A. D. & Norry, M. J. (eds) *Magmatism in the Ocean Basins. Geological Society, London, Special Publications* **42**, 71–105.

Echeverria, L. M. (1982). Komatiites from Gorgona Island, Colombia. In: Arndt, N. T. & Nisbet, E. G. (eds) *Komatiites*. London: George Allen & Unwin, pp. 199–202.

Eggins, S. M., Woodhead, J. D., Kinsley, L. P. J., Mortimer, G. E., Sylvester, P., McCulloch, M. T., Hergt, J. M. & Handler, M.R. (1997). A simple method for the precise determination of >40 trace elements in geological samples by ICPMS using enriched isotope internal standardization. *Chemical Geology* **134**, 311–326.

Ewart, A., Collerson, K. D., Regelous, M., Wendt, J. I. & Niu, Y. (1998). Geochemical evolution within the Tonga–Kermadec–Lau arc–backarc system: the role of varying mantle wedge composition in space and time. *Journal of Petrology* **39**, 331–368.

Fang, N., Ma, H., Feng, Q., Liu, B. & He, F. (1996). Late Paleozoic komatiites and oceanic island sequences in Changning–Menglian belt and their tectonic implications. In: Fang, N. & Feng, Q. (eds) *Devonian to Triassic Tethys in Western Yunnan, China*. Wuhan: China University of Geosciences Press, pp. 45–51.

Fitton, J. G., Saunders, A. D., Norry, M. J., Hardarson, B. S. & Taylor, R. N. (1997). Thermal and chemical structure of the Iceland plume. *Earth and Planetary Science Letters* **153**, 197–208.

Green, D. H., Falloon, T. J., Eggins, S. M. & Yaxley, G. M. (2001). Primary magmas and mantle temperatures. *European Journal of Mineralogy* **13**, 437–451.

Griffin, W. L., O'Reilley, S. Y. & Ryan, C. G. (1999). The composition and origin of subcontinental lithosphere. *Geochemical Society Special Publication* **6**, 13–46.

Grove, T. L., Kinzler, R. J. & Bryan, W. B. (1992). Fractionation of mid-ocean ridge basalts (MORB). In: Phipps Morgan, J., Blackman, D. K. & Sinton, J. M. (eds). *Mantle Flow and Melt Generation at Mid-ocean Ridges, Geophysical Monograph, American Geophysical Union* **71**, 281–310.

Grove, T. L., Parman, S. W. & Dann, J. C. (1999). Conditions of magma generation for Archean komatiites from the Barberton Mountainland, South Africa. *Geochemical Society Special Publication* **6**, 155–167.

Hékinian, R., Bideau, D., Herbért, R. & Niu, Y. (1995). Magmatic processes at upper mantle–crustal boundary zone: Garrett Transform (EPR South). *Journal of Geophysical Research* **100**, 10163–10185.

Herzberg, C. (1999). Phase equilibrium constraints on the formation of cratonic mantle. *Geochemical Society Special Publication* **6**, 241–258.

Herzberg, C. & O'Hara, M. J. (1998). Phase equilibrium constraints on the origin of basalts, picrites, and komatiites. *Earth-Science Reviews* **44**, 39–79.

Herzberg, C. & O'Hara, M. J. (2002). Plume-associated ultramafic magmas of Phanerozoic age. *Journal of Petrology* **43**, 1857–1883.

Hofmann, A. W. (1988). Chemical differentiation of the Earth: the relationship between mantle, continental crust, and oceanic crust. *Earth and Planetary Science Letters* **90**, 297–314.

Johum, K. P., Arndt, N. T. & Hofmann, A. W. (1991). Nb–Th–La in komatiites and basalts: constraints on komatiite petrogenesis and mantle evolution. *Earth and Planetary Science Letters* **107**, 272–289.

Kerr, A. C. & Arndt, N. T. (2001). A note on the IUGS reclassification of the high-Mg and picritic volcanic rocks. *Journal of Petrology* **42**, 2169–2171.

Kerr, A. C., Marriner, G. F., Arndt, N. T., Tarney, J., Nivia, A., Saunders, A. D. & Duncan, R. A. (1996). The petrogenesis of Gorgona komatiites, picrites and basalts: new field, petrographic and geochemical constraints. *Lithos* **37**, 245–260.

Klein, E. M. & Langmuir, C. H. (1987). Global correlations of ocean ridge basalt chemistry with axial depth and crustal thickness. *Journal of Geophysical Research* **92**, 8089–8115.

Kwiecien, W. (1990). *Silicate Rock Analysis by AAS*. Brisbane School of Geology, Queensland University Technology.

Langmuir, C. H. & Hanson, G. N. (1981). Calculating mineral–melt equilibria with stoichiometry, mass balance, and single-component distribution coefficients. In: Newton, R. C., Navrotsky, A. & Wood, B. J. (eds) *Thermodynamics of Minerals and Melts*. New York: Springer, pp. 247–271.

Langmuir, C. H., Klein, E. M. & Plank, T. (1992). Petrological systematics of mid-ocean ridge basalts: constraints on melt generation beneath ocean ridges. In: Phipps Morgan, J., Blackman, D. K. & Sinton, J. M. (eds). *Mantle Flow and Melt Generation at Mid-ocean Ridges. Geophysical Monograph, American Geophysical Union* **71**, 183–280.

Le Bas, M. J. (2000). IUGS reclassification of the high-Mg and picritic volcanic rocks. *Journal of Petrology* **41**, 1467–1470.

Le Bas, M. J. (2001). Reply to comments by Kerr and Arndt. *Journal of Petrology* **42**, 2173–2174.

McDonough, W. F. & Ireland, T. R. (1993). Intraplate origin of komatiites inferred from trace elements in glass inclusions. *Nature* **365**, 432–434.

McKenzie, D. & Bickle, M. J. (1988). The volume and composition of melt generated by extension of the lithosphere. *Journal of Petrology* **29**, 625–679.

Nielson, R. L. & Dungan, M. A. (1983). Low pressure mineral–melt equilibria in natural anhydrous mafic systems. *Contributions to Mineralogy and Petrology* **84**, 310–326.

Nisbet, E. G. (1982). The tectonic setting and petrogenesis of komatiites. In: Arndt, N. T. & Nisbet, E. G. (eds) *Komatiites*. London: George Allen & Unwin, pp. 501–520.

Nisbet, E. G., Cheadle, M. J., Arndt, N. T. & Bickle, M. J. (1993). Constraining the potential temperature of the Archean mantle: a review of the evidence from komatiites. *Lithos* **30**, 291–307.

Niu, Y. (1997). Mantle melting and melt extraction processes beneath ocean ridges: evidence from abyssal peridotites. *Journal of Petrology* **38**, 1047–1074.

Niu, Y. & Batiza, R. (1991). An empirical method for calculating melt compositions produced beneath mid-ocean ridges: application for axis and off-axis (seamounts) melting. *Journal of Geophysical Research* **96**, 21753–21777.

Niu, Y. & Batiza, R. (1997). Trace element evidence from seamounts for recycled oceanic crust in the eastern Pacific mantle. *Earth and Planetary Science Letters* **148**, 471–483.

Niu, Y., Collerson, K. D., Batiza, R., Wendt, J. I. & Regelous, M. (1999). The origin of E-Type MORB at ridges far from mantle plumes: the East Pacific Rise at 11°20′N. *Journal of Geophysical Research* **104**, 7067–7087.

Niu, Y., Bideau, D., Hékinian, R. & Batiza, R. (2001). Mantle compositional control on the extent of melting, crust production, gravity anomaly and ridge morphology: a case study at the Mid-Atlantic Ridge 33–35°N. *Earth and Planetary Science Letters* **186**, 383–399.

Niu, Y., Gilmore, T., Mackie, S., Greig, A. & Bach, W. (2002*a*). Mineral chemistry, whole-rock compositions and petrogenesis of ODP Leg 176 gabbros: data and discussion. In: Natland, J.H., Dick H.J.B., Miller, D.J. & Von Herzen, R.P. (eds) *Proceedings of Ocean Drilling Program Scientific Results, 176*. College Station, TX: Ocean Drilling Program, pp. 1–60. [On line.] Available at: http://wwwodp.tamu.edu/publications/176_SR/VOLUME/CHAPTERS/SR176_08.PDF.

Niu, Y., Regelous, M., Wendt, J. I., Batiza, R. & O'Hara, M. J. (2002*b*). Geochemistry of near-EPR seamounts: importance of *source* vs. *process* and the origin of enriched mantle component. *Earth and Planetary Science Letters* **199**, 327–345.

Parman, S. W., Dann, J. C., Grove, T. L. & de Wit, M. J. (1997). Emplacement conditions of komatiite magmas from the 3·49 Ga Komati Formation, Barberton Greenstone belt, South Africa. *Earth and Planetary Science Letters* **150**, 303–323.

Pearce, J. A. & Peate, D. W. (1995). Tectonic implications of the composition of volcanic arc magmas. *Annual Review of Earth and Planetary Sciences* **23**, 251–285.

Regelous, M., Niu, Y., Wendt, J. I., Batiza, R., Greig, A. & Collerson, K.D. (1999). An 800 ka record of the geochemistry of magmatism on the East Pacific Rise at 10°30′N: insights into magma chamber processes beneath a fast-spreading ocean ridge. *Earth and Planetary Science Letters* **168**, 45–63.

Renner, R. (1989). Cooling and crystallization of komatiite flows from Zimbabwe. Ph.D. Thesis, University of Cambridge, 162 pp.

Révillon, S., Arndt, N. T., Chauvel, C. & Hallot, E. (2000). Geochemical study of ultramafic volcanic and plutonic rocks from Gorgona Island, Colombia: the plumbing system of an oceanic plateau. *Journal of Petrology* **41**, 1127–1153.

Richter, F. M. (1988). A major change in the thermal state of the Earth at the Archean–Proterozoic boundary: consequences for the nature and preservation of continental lithosphere. *Journal of Petrology Special Lithosphere Issue* 39–52.

Roeder, P. L. & Emslie, R. F. (1970). Olivine–liquid equilibrium. *Contributions to Mineralogy and Petrology* **29**, 275–289.

Rudnick, R. L. & Fountain, D. M. (1995). Nature and composition of the continental crust: a lower crustal perspective. *Reviews of Geophysics* **33**, 267–309.

Stone, W. E., Deloule, E., Larson, M. S. & Lesher, C. M. (1997). Evidence for hydrous high-MgO melts in the Precambrian. *Geology* **25**, 143–146.

Sun, S.-s. & McDonough, W. F. (1989). Chemical and isotopic systematics in ocean basalt: implication for mantle composition and processes. In: Saunders, A. D. & Norry, M. J. (eds) *Magmatism in the Ocean Basins. Geological Society, London, Special Publications* **42**, 313–345.

Sylvester, P. J., Campbell, I. H. & Bowyer, D. A. (1997). Niobium/uranium evidence for early formation of the continental crust. *Science* **275**, 521–523.

Sylvester, P. J., Kamenetsky, V. S. & McDonough, W. F. (2000). Melt inclusion evidence for komatiite genesis in Gorgona plume. *Journal of Conference Abstracts* **5**, 957.

Walker, D., Shibata, T. & De Long, S. E. (1979). Abyssal tholeiites from the Oceanographer Fracture Zone, II, Phase equilibria and mixing. *Contributions to Mineralogy and Petrology* **70**, 111–125.

Wang, H. Z. & Mo, X. X. 1995. An outline of tectonic evolution of China. *Episodes* **18**, 6–16.

Weaver, J. S. & Langmuir, C. H. (1990). Calculations of phase equilibrium in mineral–melt systems. *Computers and Geosciences* **16**, 1–19.